A Microfabricated 8-40 GHz Dual-Polarized Reflector Feed

Kenneth Vanhille[1], Tim Durham[2], William Stacy[1], David Karasiewicz[1], Aaron Caba[1], Christopher Trent[2], Kevin Lambert[3], and Félix Miranda[4]

[1]Nuvotronics, LLC, Durham, NC 27703
[2]Harris Corporation, Melbourne, FL 32902
[3]Vantage Partners, LLC, Cleveland, OH, 44135
[4]NASA Glenn Research Center, Cleveland, OH 44135

Abstract: Planar antennas based on tightly coupled dipole arrays (also known as a current sheet antenna or CSA) are amenable for use as electronically scanned phased arrays. They are capable of performance nearing a decade of bandwidth. These antennas have been demonstrated in many implementations at frequencies below 18 GHz. This paper describes the implementation using a relatively new multi-layer microfabrication process resulting in a small, 6x6 element, dual-linear polarized array with beamformer that operates from 8 to 40 GHz. The beamformer includes baluns that feed the dual-polarized differential antenna elements and reactive splitter networks that also cover the full frequency range of operation. This antenna array serves as a reflector feed for a multi-band instrument designed to measure snow water equivalent (SWE) from airborne platforms. The instrument has both radar and radiometry capability at multiple frequencies. Scattering-parameter and time-domain measurements have been used to characterize the array feed. Radiation patterns of the antenna have been measured and are compared to simulation. To the best of the authors' knowledge, this work represents the most integrated multi-octave millimeter-wave antenna feed fabricated to date.

1. Introduction

The National Research Council releases a decadal survey identifying the highest-priority space-based earth science missions. An interim report from the committee identified snow water equivalent (SWE) as an important parameter to understand the global hydrological cycle [1]. This is important for water resource management for many areas of the world, including the Western United States. Spatial and temporal snow information is lacking—mainly provided by sparse *in-situ* sensors or infrequent aircraft observations. The NASA Snow and Cold Land Processes (SCLP) Earth science mission is a future mission defined to provide the satellite-based capability to perform such

measurements. Specifically, the SCLP concept calls for a combination of synthetic aperture radar and radiometry over a broad band of frequencies between the X- and Ka-bands. The authors have been part of a team that has concentrated on maturing technology that would demonstrate the capability sought for this mission in anticipation of an opportunity to address the science objectives [2]. This demonstration involves the development of a Wideband Instrument for Snow Measurements (WISM), which is a multi-band instrument that provides both radar and radiometry capability from X- to Ka-band frequencies. The antenna is a reflector that is fed with a wideband, dual-polarized feed that operates from 8 to 40 GHz in a co-boresighted fashion.

Wideband phased arrays have been of great interest in recent years [3]. A variety of planar antennas such as the fragmented aperture antenna [4] have been demonstrated. The current sheet antenna has been patented and developed at Harris Corporation [5]. Multi-octave frequency performance has been shown using this design technique. The current sheet array achieves near decade bandwidth by controlling the mutual coupling between elements in such a way that the active impedance is relatively constant. This is in opposition to previously utilized approaches where a wide bandwidth element in isolation was put into an array only to have the bandwidth severely reduced by mutual coupling. Emerging fabrication technologies provide the possibility of moving such antenna designs to millimeter-wave frequencies where traditional fabrication capabilities have proven limited. One such emerging technology is the PolyStrata® fabrication process [6], which is a wafer-scale, batch fabrication technique that provides structures with 15 or more independently-defined 'strata' with the intralayer ability to precisely define regions of metal (generally copper), photo-patternable permanent dielectric and air. These structures are generally monolithically fabricated with a total thickness of up to 1 mm (although more than double that thickness has been demonstrated), and then stacked to achieve higher numbers of layers. As a transmission line, losses achieved are 2X-10X lower than what is typical with common planar transmission line media such as microstrip, co-planar waveguide or stripline. This is by virtue of the fact that these rectangular coaxial transmission lines are primarily air loaded. This decreases the dielectric loss, and decreases the effective dielectric constant which in turn increases the size of the signal trace (also decreasing the loss) [7]. In addition to transmission lines, a wide variety of filters, antennas, baluns and other microwave structures have been demonstrated using this technology. Specifically, frequency independent antennas such as log-periodic antennas have been demonstrated using the PolyStrata technology [8]; however, antennas capable of implementation in an array environment have not been previously shown.

The outline of the remainder of the paper is as follows. Section 2 describes the architecture of the antenna feed. Section 3 provides performance results of some of the building blocks that make up the antenna feed. Section 4 provides measured results for the full antenna feed. Measured and simulated radiation patterns are included in addition to scattering parameters of the antenna feed. Section 5 provides a summary of the results presented in this paper with a brief indication of future work.

2. Architecture Design

The WISM antenna feed is constructed of multiple instances of several fundamental microwave building blocks. A block diagram of the full antenna feed is shown in Figure 1 with blocks representing each of the nine 2x2 sub-array modules (hereafter simply referred to as modules) that make up the model and two blocks that represent the initial layer of splitter networks that configures the performance of the array. Figure 2 shows a pictorial representation of the block diagram shown in Figure 1. In the configuration implemented for WISM, the four corner modules are combined in phase with the assumption that they will be used for X-band frequencies (labeled X1, X2, X3, and X4 in Figure 1). The center cross of modules is combined with the center module (labeled AA1) receiving half of the energy and the other four modules receiving one eighth of the power (AA2, AA3, AA4 and AA5). These modules are used for the Ku- and Ka-band frequencies of operation. This separation of the frequencies is done to reduce the variation in illumination taper on the reflector versus frequency thereby reducing the change in secondary pattern beamwidth. All the modules individually are capable of operating over the full frequency range. Figure 3 shows greater detail regarding any one of the nine modules.

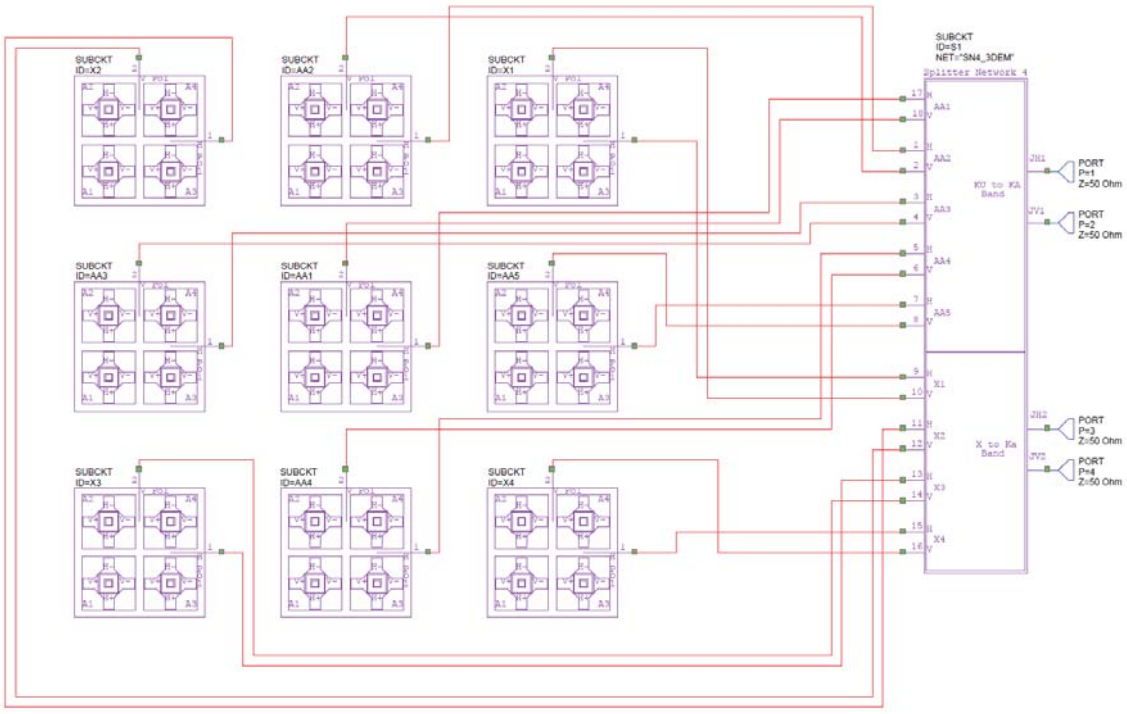

Figure 1. The block diagram of the 6x6 element WISM antenna feed. Each of the nine building blocks is a 2x2 element sub-array, as detailed in Figure 3. At right is a representation of the final combining networks that sets the radiation characteristics of the antenna. By reconfiguring this final combining network, other possible illumination schemes are possible.

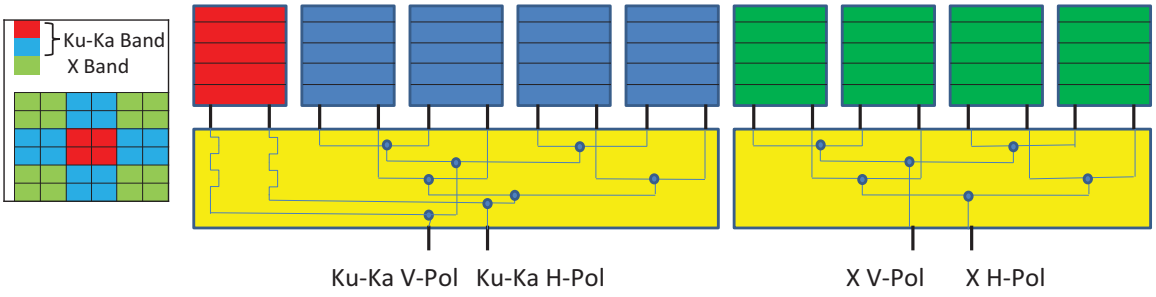

Figure 2. Pictorial representation of the feed network shown in the block diagram of Figure 1.

For the initial demonstration, there are two radar bands and two radiometry bands. The general frequency bands are shown in Table 1. One advantage of the broadband antenna feed is that additional or different bands can be added, depending on the application without having to design and build a new antenna. Current plans call for adding additional frequency bands to the instrument as part of a follow-on effort to the original IIP.

Table 1. The frequency bands of operation for the WISM antenna.

Function	F_{low} (GHz)	F_{high} (GHz)	Array Portion
Active Radar	9.5	9.8	X-Band
Active Radar	17.2	17.3	Ku/Ka-Band
Passive Radiometer	18.6	18.9	Ku/Ka-Band
Passive Radiometer	36.0	37.0	Ku/Ka-Band

The 2x2 antenna module is dual polarized and each element is differentially fed, so there are 16 RF connectors to the antennas in each module. Two-way splitters are located behind each element to combine pairs of elements. Baluns then combine the differential lines for each pair of elements. A final splitter combines the single-ended signals for each pair of elements, leaving one port for each radiation polarization. Physically, these functions are divided across four PolyStrata devices, as indicated by the objects labeled SN1, SN2, Balun, and SN3 in the block diagram of Figure 3. In SN1, the horizontally-polarized signals combine in a two-way splitter and then pass through the next layer; the vertically-polarized signals pass through SN1 without modification. In SN2, the vertically polarized signals are combined in two-way splitters and pass to the Balun device; the horizontally polarized signals pass through SN2. In the Balun device, four baluns combine four pairs of differential signals into two signals for each polarization. In SN3 there is a final set of splitter networks that combines the signals for each polarization, providing one port on the bottom of the module for each polarization.

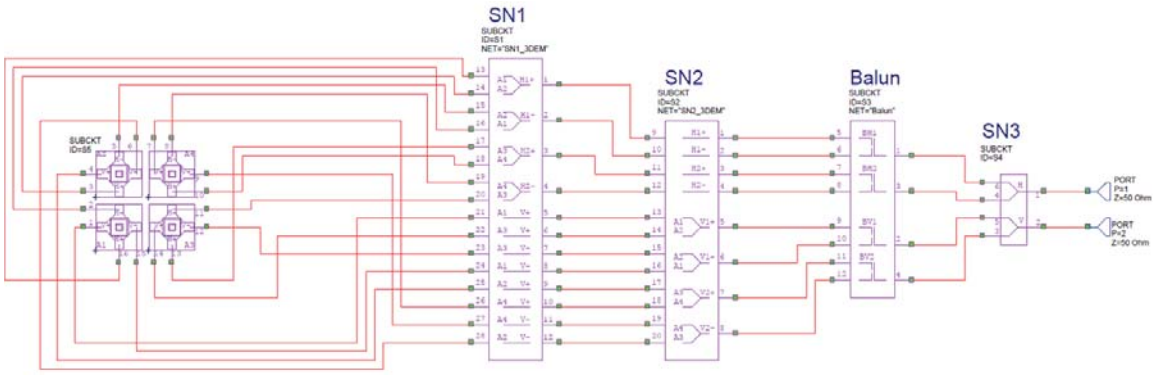

Figure 3. The block diagram of a 2x2 element sub-array that constitutes the building block for the 6x6 array shown in Figure 1.

3. Component Performance

The feed design described in the previous section uses several components as the base building blocks. These components include current sheet antenna radiating elements, baluns, splitter networks, vertical transitions, and transitions to standard 2.4mm connectors. They have each been designed, fabricated, and tested as described in the remainder of the section. The simulations were performed using a three-dimensional finite element method software package, ANSYS® HFSS™.

A balun is able to convert a *bal*anced signal to an *un*balanced signal. Many types of baluns exist, although the topologies presented by Marchand [9] have gained common usage. Such a balun design is used to convert the single-ended feed to the differentially-driven CSA elements. A circuit diagram is shown at left in Figure 4 with a 3-D model of the electrical implementation shown at right. The transmission lines 'a' and 'b' are routed in a cavity where the outer conductor of these transmission lines forms the center conductor of the 'ab' transmission lines with the cavity walls at the ground potential. The outer conductors of 'a' and 'b' are connected to the center conductors of the two 'c' lines going to ports 2 and 3. Using such a topology, a 5:1 frequency bandwidth is achievable from 8 to 40 GHz. Two styles of test pieces were fabricated and tested using ground-signal-ground (GSG) probes on a two-port vector network analyzer. One is a back-to-back balun to provide a loss measurement and the other is a three-port device where the differential ports are separate 50-Ohm ports that can be GSG probed using a similar configuration to the single-ended port. For measurements, the third port of the single test balun was loaded with a coaxial termination on a microwave probe. The termination was not de-embedded from the measurement. This non-ideal termination of the third port causes the ripple seen in the measured results of the magnitude of S_{11}, S_{21} and S_{31}. The measurements were calibrated using a set of TRL calibration standards with similar probe interface ports fabricated using the PolyStrata® fabrication process. This balun has a maximum measured VSWR of 2:1 over the frequency range, and the S_{11} in dB is plotted

in Figure 5. Figure 6 shows the measured versus simulated S_{21} and S_{31} in dB going through the balun. The phase difference in degrees between the two paths is shown in Figure 7. The phase imbalance is less than 10 degrees over the frequency band and the amplitude imbalance is 0.2 dB over the frequency band except for near 9 GHz where the measurement calibration does not look ideal. The balun performance is adequate for the reflector feed application. The size of the balun test device is 9mm by 8mm; however the actual balun is 3.5mm by 5.5mm.

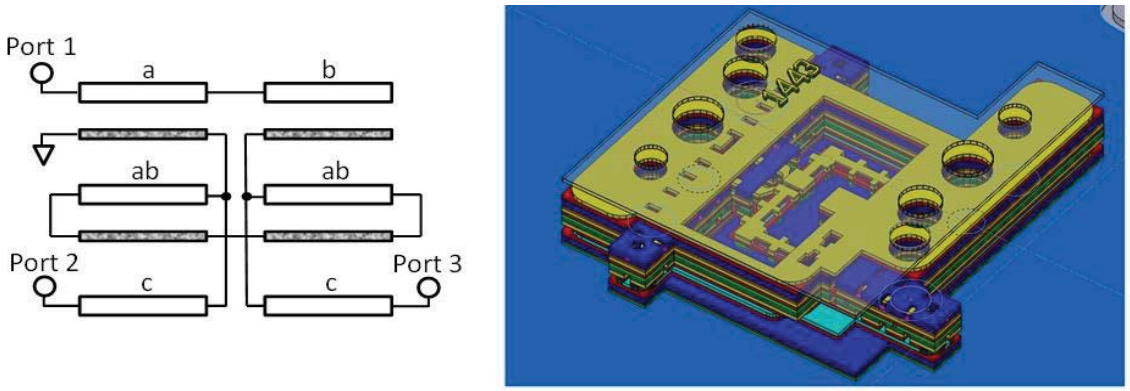

Figure 4. (left) Circuit diagram of the balun topology employed. (right) 3-D model of the single-balun test piece. The top of the cavity is transparent. The microwave-probe landing interfaces are visible in the lower right (Port 1), lower left (Port 2), and upper (Port 3) regions of the image.

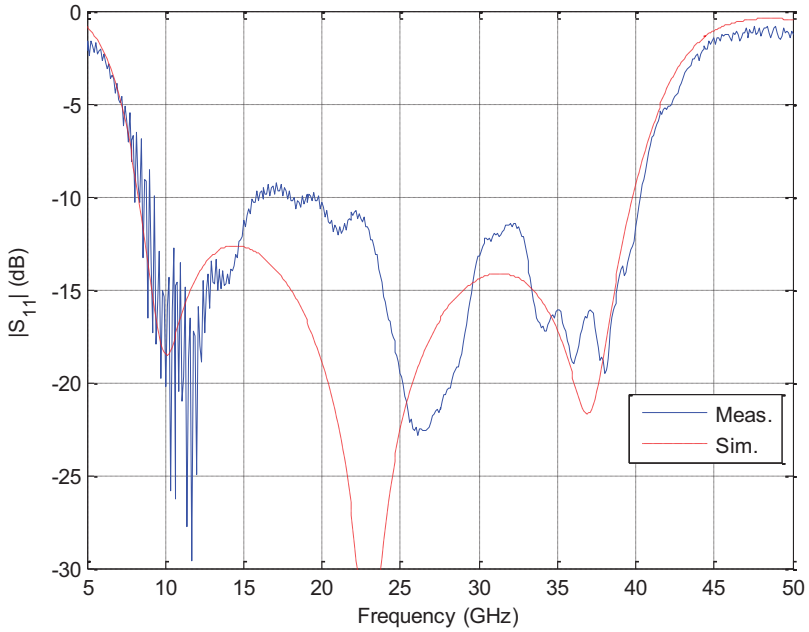

Figure 5. Measured versus simulated $|S_{11}|$ performance in dB of the single balun test structure.

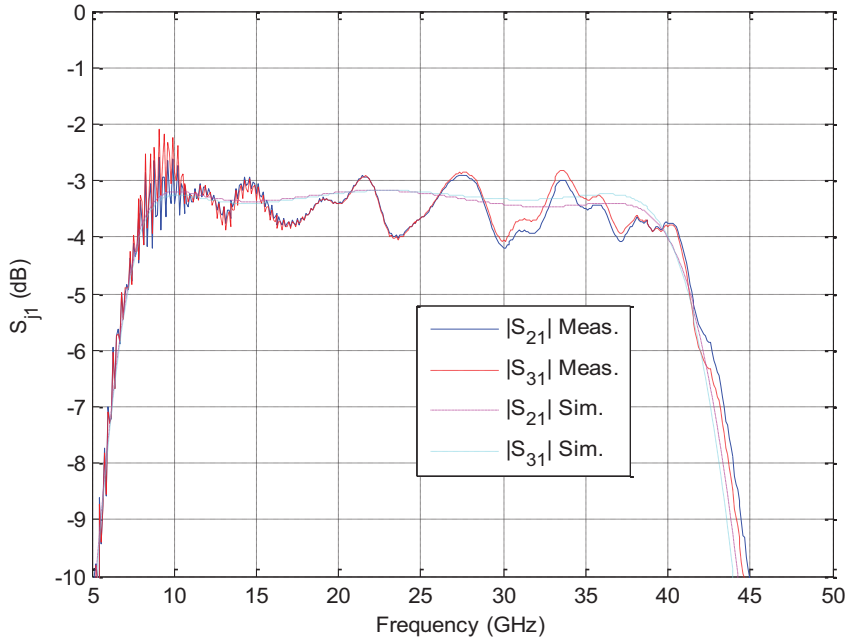

Figure 6. Measured versus simulated $|S_{21}|$ and $|S_{31}|$ performance in dB of the balun test structure.

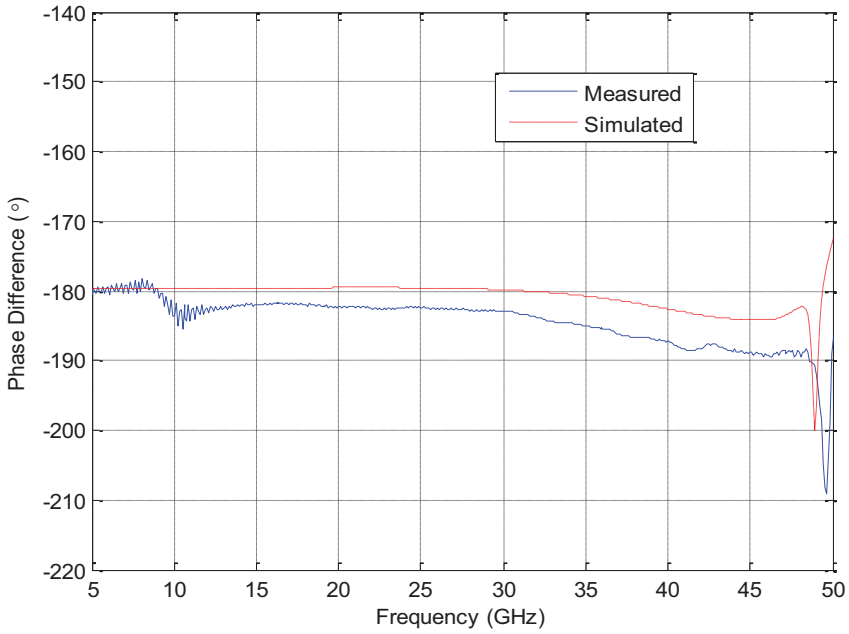

Figure 7. Measured versus simulated phase difference between S_{21} and S_{31} in degrees of the balun test structure.

Another building-block component that is required for the reflector feed is a reactive splitter that also operates over the 8-40 GHz frequency range. A splitter test component was fabricated to provide confidence that similar designs will operate as expected in the full antenna assembly. An image of a back-to-back version of the splitter that provides a loss estimate is shown at left in Figure 8. The measured versus simulated performance is shown at right in Figure 8.

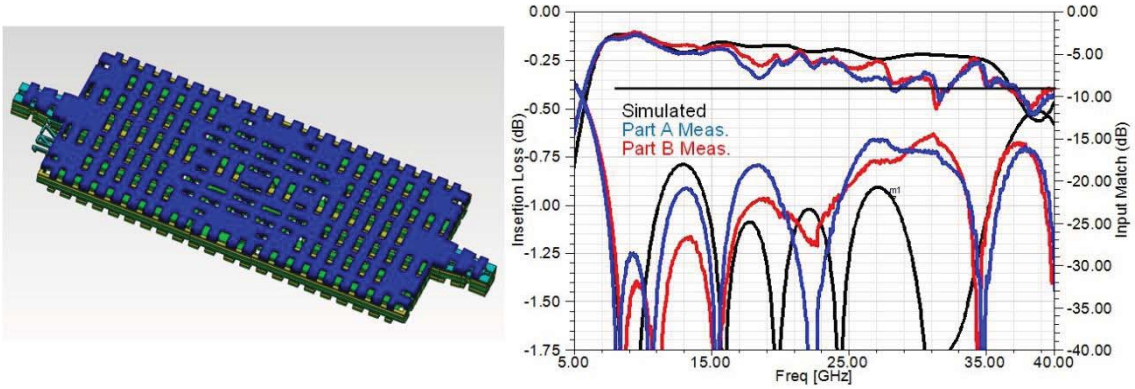

Figure 8. (left) 3-D model of 8-40 GHz splitter test device. (right) Measured versus simulated performance for two separate splitter test devices.

The power handling of rectangular coaxial transmission lines that go between multiple layers and for transmission lines that have methods of removing the heat from the center conductor are published in [10]. This content of the paper is not exhaustive, but it provides an understanding of what may be possible using the rectangular coaxial transmission lines. It was shown that >200 W at 2 GHz can be passed through rectangular coaxial lines of a cross section of roughly 700 μm on a side if adequate methods of removing the heat from the center conductor are available. It was also shown that a similar power level is achievable in the same cross section transmission line at a simulated elevation of > 9000 m above sea level.

4. Measurements

A photograph of the WISM antenna feed is shown in Figure 9. The antenna consists of nine (9) 2x2 element building blocks in a 3x3 grid to make a total of 36 dual-polarized antenna elements. Each element is differentially fed. Four 2.4mm connectors are attached to the backside of the antenna. Two connectors provide vertical and horizontal polarization for the portion of the array fed with Ku- through Ka-band frequencies. Two connectors provide vertical and horizontal polarization for the portion of the array fed with X-band frequencies. Although the array is capable of wideband operation over the full frequency range, different portions of the array are fed at different frequencies to approximately equalize the beamwidth of the radiation from the array over frequency.

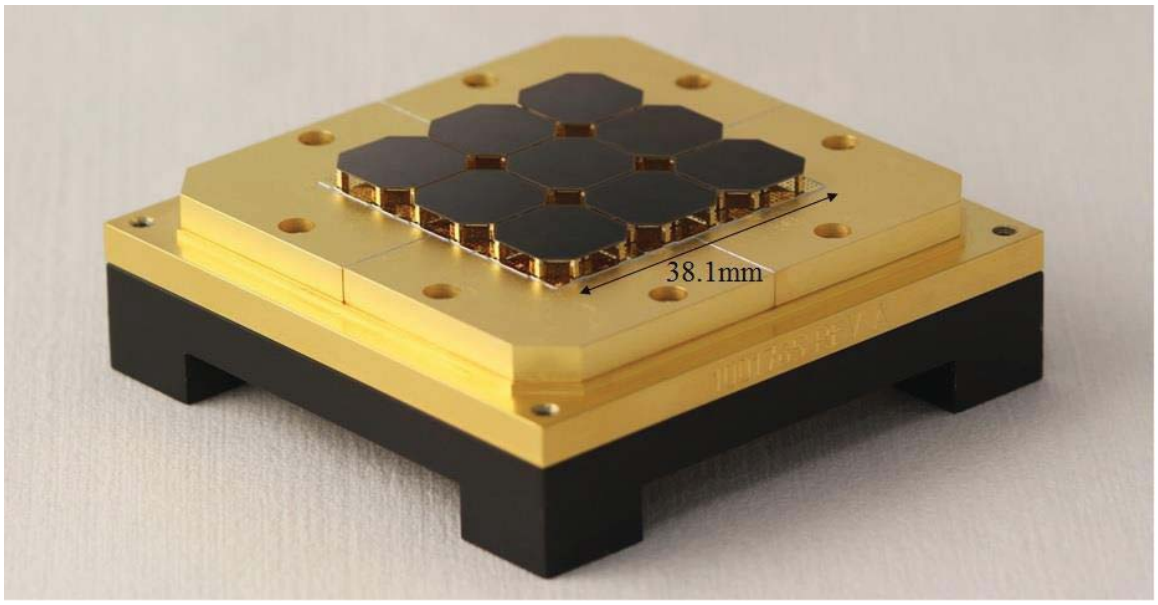

Figure 9. Photograph of the final WISM antenna feed. The outer dimensions of the antenna are 71.1mm by 71.1mm, although the PolyStrata® portion is 38.1mm on a side.

A photograph of one 2x2 sub-array module is shown in Figure 10. This sub-array module consists of six separate pieces that have been fabricated using the PolyStrata® technology which are then stacked together to provide the necessary performance for the sub-array. The block diagram for the functionality of a given sub-array module is shown in Figure 3. Within the 12.7mm by 12.7mm sub-array module there are four (4) baluns, ten (10) splitters, 24 layer to layer transitions—all of the components operate over the 8-40 GHz frequency range.

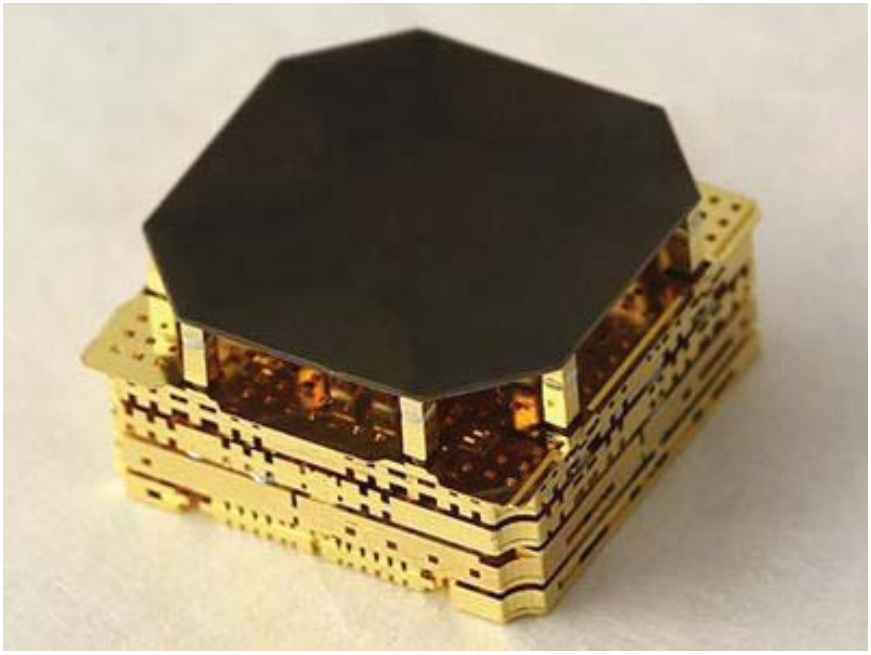

Figure 10. A photograph of the 2x2 element sub-array whose block diagram is shown in Figure 3.

To focus on the performance of the antenna array beam-forming network, a measurement was conducted that uses time gating to remove the reflections caused by the radiating elements. These measurements are compared with a circuit model that uses cascaded scattering parameter blocks for each of the full-wave models that were simulated for antenna array. Figure 11 shows the performance of the Ku-Ka-band feed network for the vertical polarized antenna. Figure 12 shows the scattering parameter performance of the X-band feed network for the vertical polarized portion of the array.

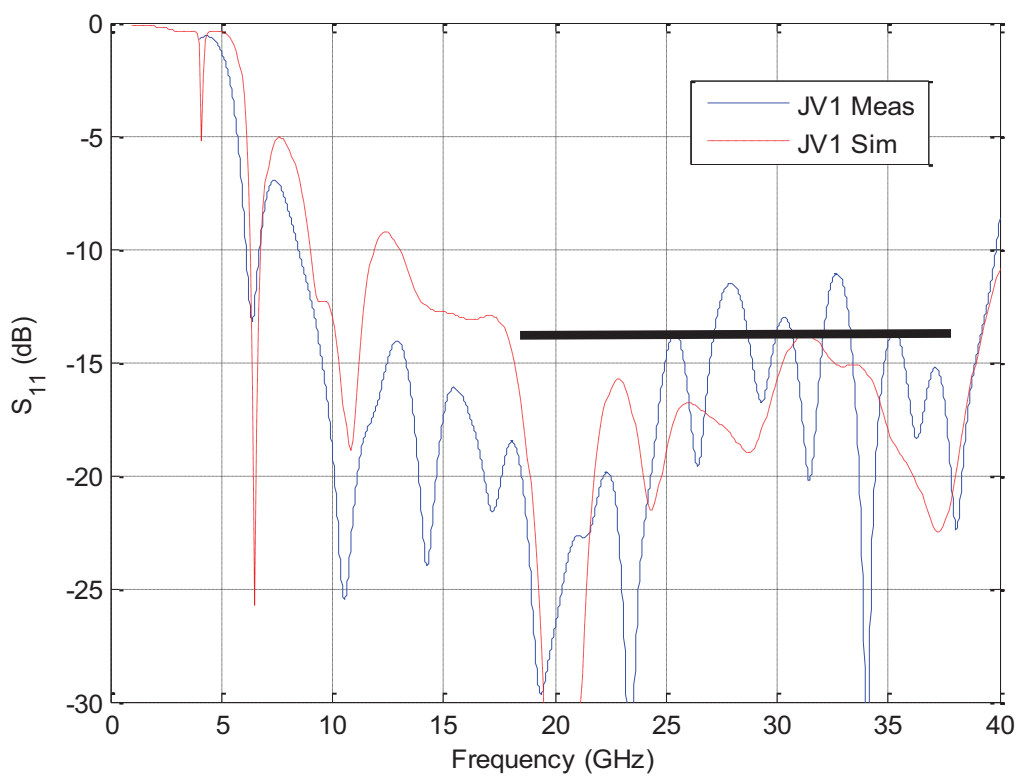

Figure 11. The measured versus simulated performance of the beam-forming network for the Ku-Ka-band portion of the array for the vertical polarization. The radiating elements are time-gated out to focus on the feed network performance.

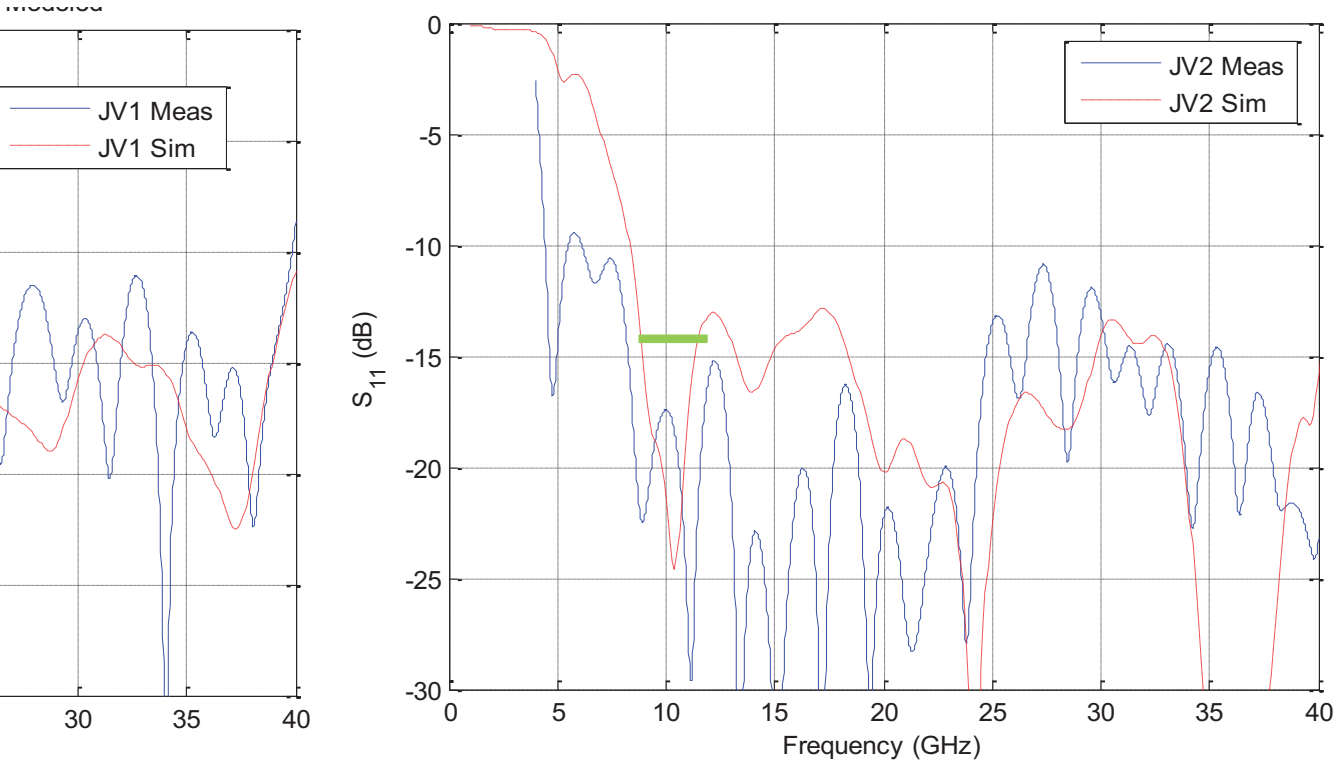

Figure 12. The measured versus simulated performance of the beam-forming network for the X-band portion of the array for the vertical polarization. The radiating elements are time-gated out to focus on the feed network performance.

The antenna was measured at the NASA Glenn Research Center (GRC) in an anechoic chamber, as shown in Figure 13 (an earlier version of the antenna is shown). This antenna has only a single 2x2-element sub-array module as an intermediate hardware demonstration prior to fabrication of the full array, however a similar setup was used to measure the radiation patterns of the hardware shown in Figure 9. Both co-polarized and cross-polarized measurements were taken at multiple frequencies. A summary of the results is presented here. Radiation pattern measurements at or near each of the frequency bands identified in Table 1 are shown. The vertical polarization is co-polarized in the azimuth = 0° direction. The horizontal polarization is co-polarized in the azimuth = 90° direction. Figure 14 shows the measured versus modeled performance of the antenna feed in the inter-cardinal plane at the Ku/Ka-band vertically-polarized port at 36.5 GHz. Figure 15 shows the measured performance of the vertically-polarized antenna feed at 9.75 GHz when excited at the X-band port for *az*=0°. Figure 16 shows the measured performance of the Ku/Ka-band portion of the vertically-polarized antenna feed at 17.2 GHz. Finally, Figure 17 shows the measured performance of the Ku/Ka-band portion of the horizontally-polarized antenna feed at 18.5 GHz for *az*=90°. In each of the cases presented, the cross-polarization isolation is greater than 30 dB over an angular region greater than the 3-dB beamwidth of the antenna.

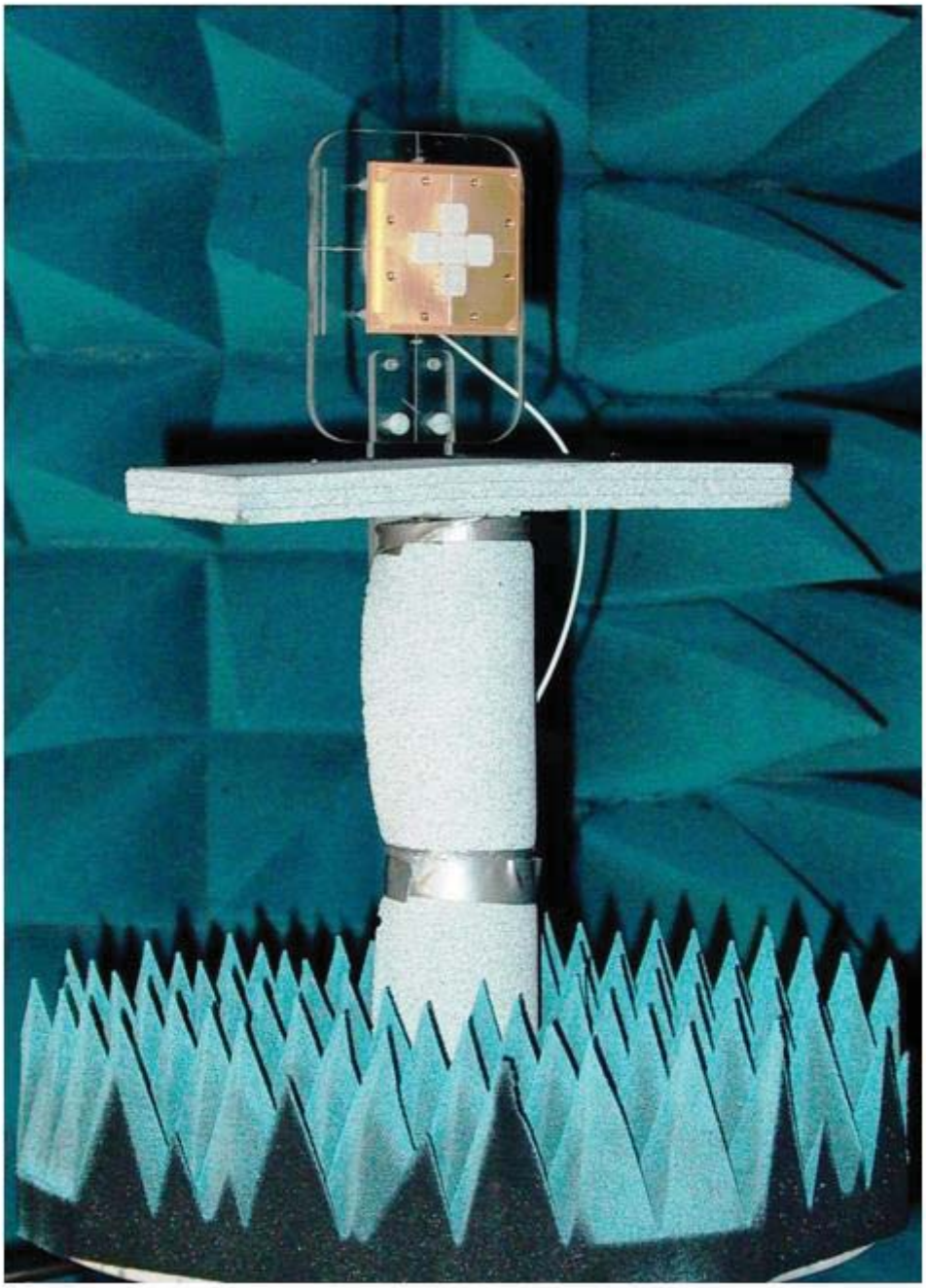

Figure 13. A photograph of an earlier version of the WISM reflector feed at the Glenn Research Center (GRC) antenna test facility.

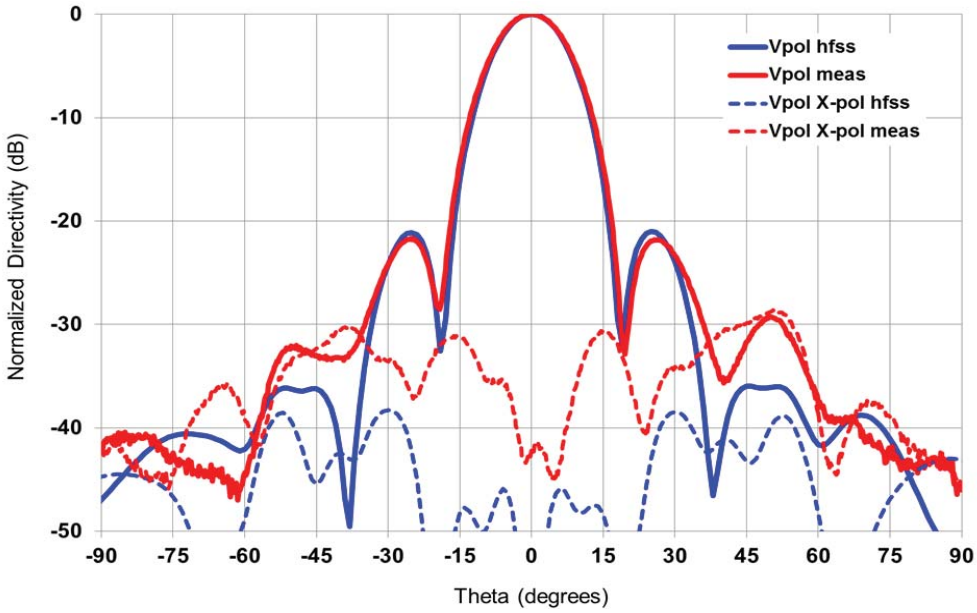

Figure 14. The measured versus simulated performance at 36.5 GHz for the vertically-polarized portion of the Ku/Ka-band portion of the array at an azimuth angle of 45°.

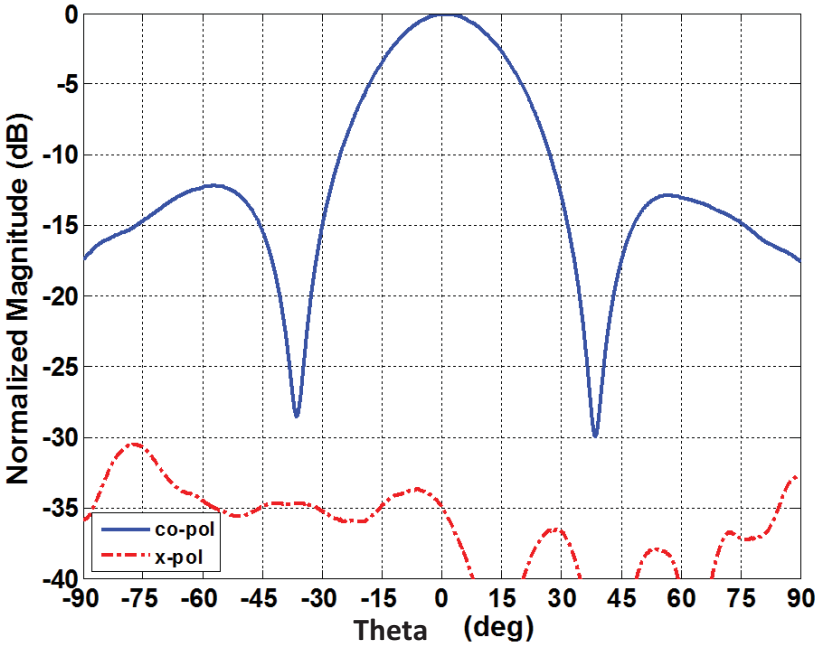

Figure 15. The measured co-polarized and cross-polarized performance at 9.75 GHz at an azimuth angle of 0° for the X-band vertically-polarized portion of the array.

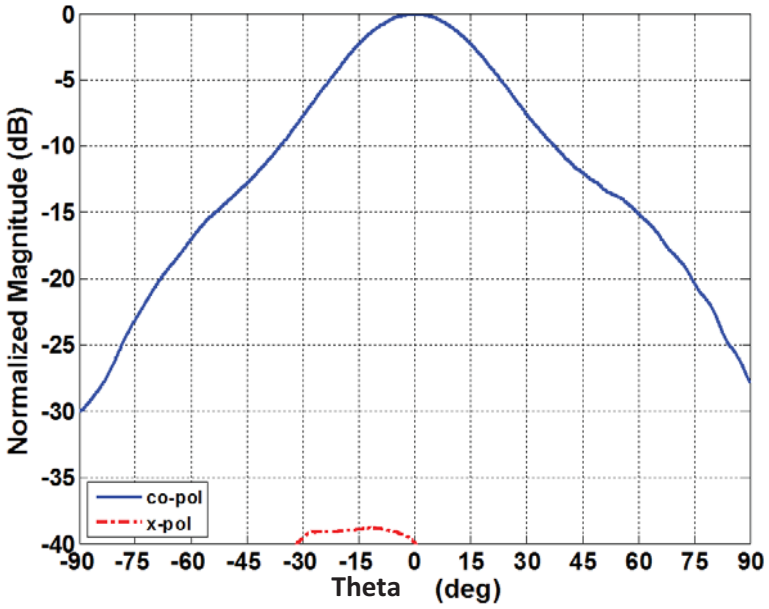

Figure 16. The measured co-polarized and cross-polarized performance at 17.2 GHz at an azimuth angle of 0° for the Ku/Ka-band vertically polarized portion of the array.

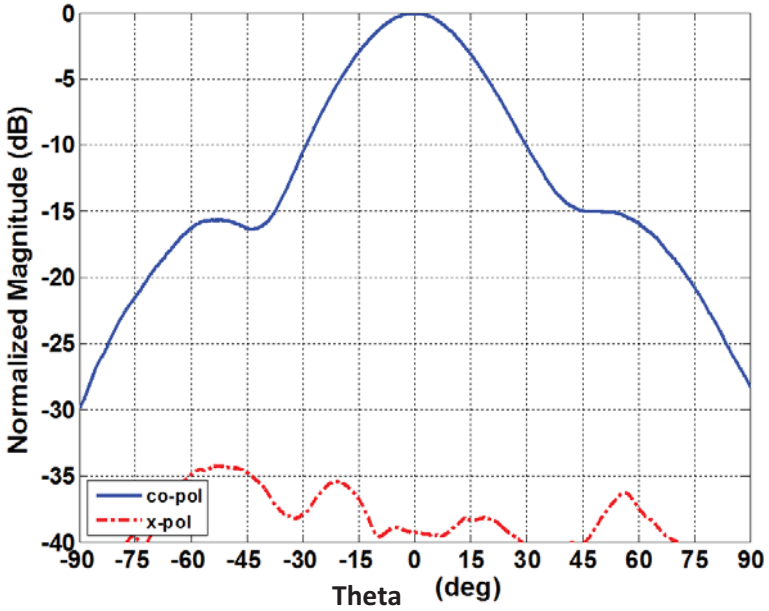

Figure 17. The measured co-polarized and cross-polarized performance at 18.5 GHz at an azimuth angle of 90° for the Ku/Ka-band horizontally polarized portion of the array.

5. Summary

A wideband reflector antenna feed that is capable of millimeter-wave operation has been designed, fabricated and tested. This feed demonstrates the integration capability of the PolyStrata technology and shows a possible approach to integrating co-boresighted multi-band instruments for future satellite-based earth science missions. A version of the antenna has been used for ground-based snow radar measurements. Future work is planned to demonstrate the current instrument over a series of airborne measurement campaigns, increase the number of radar and radiometer bands for the instrument, and decrease the feed loss.

There is a high degree of flexibility with the design architecture approach as it is described in Section 2. Each module may be capable of operating over the entire frequency range. Depending on how the modules are tied together, different field patterns can be obtained to illuminate the reflector. The modules represent re-usable design building blocks that may be used to create larger arrays. In addition, the modules could be made active by embedding low noise amplifiers (LNAs) or other electronic components for improved noise figure, electronic scanning, etc. This approach represents a compelling method of fabricating wideband antenna arrays that are planar for frequencies above 18 GHz—removing many of the integration challenges associated with Vivaldi-type antennas, especially when dual polarization is required.

6. Acknowledgment

The authors would like to thank the PolyStrata® fabrication team at Nuvotronics who manufactured the components used to create the antenna. This work was supported by grant NNX11AF27G under the Instrument Incubator Program from the Earth Science Technology Office of the National Aeronautics and Space Agency.

7. References

[1] National Academy of Sciences National Research Council, "Earth Science and Applications from Space: Urgent Needs and Opportunities to Serve the Nation Committee on Earth Science and Applications from Space: A Community Assessment and Strategy for the Future," 2005.

[2] T. Durham, H. P. Marshall, L. Tsang, P. Racette, Q. Bonds, F. Miranda and K. Vanhille, "Wideband Sensor Technologies for Measuring Surface Snow," Earthzine, 02 Dec. 2013. [Online]. Available: http://www.earthzine.org/2013/12/02/wideband-sensor-technologies-for-measuring-surface-snow/. [Accessed 18 08 2014].

[3] W. F. Croswell, T. Durham, M. Jones, D. Schaubert, P. Friederich and J. G. Maloney, "Wideband Arrays," in Modern Antenna Handbook, Hoboken, NJ, USA, Wiley & Sons, Inc., 2007.

[4] J. G. Maloney, P. H. Harms, M. P. Kesler, T. L. Fontain and G. S. Smith, "Planar antennas designed using the genetic algorithm," in USNC/URSI Radio Science Meeting, Orlando, 1999.

[5] R. C. Taylor, B. A. Munk and T. E. Durham, "Wideband Phased Array Antenna and Associated Methods". United States of America Patent 6512487B1, 28 January 2003.

[6] Z. Popovic, D. Filipovic, S. Rondineau, D. Sherrer, C. Nichols, J.-M. Rollin and K. Vanhille, "An enabling new 3D architecture for microwave components and systems," Microwave Journal, pp. 66-86, 2008.

[7] S. Huettner, "High Performance 3D Micro-Coax Technology," Microwave Journal, 2013.

[8] J. Mruk, N. Sutton and D. S. Filipovic, "Micro-Coaxial Fed 18 to 110 GHz Planar Log-Periodic Antennas with RF Transitions," IEEE Transactions on Antennas and Propagation, vol. 62, no. 2, pp. 968-972, 2014.

[9] N. Marchand, "Transmission-line Conversion Transformers," Electronics, vol. 17, no. 12, pp. 142-145, 1944.

[10] P. Ralston, K. Vanhille, A. Caba, M. Oliver and S. Raman, "Test and verification of micro coaxial line power performance," in IEEE MTT-S Int. Microwave Symposium, Montreal, Canada, 2012.